

# Hybrid Kinetics Embedding Framework for Dynamic PET Reconstruction

Yubo Ye<sup>1</sup>, Huafeng Liu<sup>1,3,4</sup> (✉), and Linwei Wang<sup>2</sup>

<sup>1</sup> State Key Laboratory of Modern Optical Instrumentation,  
Department of Optical Engineering, Zhejiang University, Hangzhou 310027, China  
liuhf@zju.edu.cn

<sup>2</sup> Rochester Institute of Technology, Rochester, NY 14623, USA

<sup>3</sup> Jiaxing Key Laboratory of Photonic Sensing & Intelligent Imaging,  
Jiaxing 314000, China

<sup>4</sup> Intelligent Optics & Photonics Research Center, Jiaxing Research Institute,  
Zhejiang University, Jiaxing 314000, China

**Abstract.** In dynamic positron emission tomography (PET) reconstruction, the importance of leveraging the temporal dependence of the data has been well appreciated. Current deep-learning solutions can be categorized in two groups in the way the temporal dynamics is modeled: data-driven approaches use spatiotemporal neural networks to learn the temporal dynamics of tracer kinetics from data, which relies heavily on data supervision; physics-based approaches leverage *a priori* tracer kinetic models to focus on inferring their parameters, which relies heavily on the accuracy of the prior kinetic model. In this paper, we marry the strengths of these two approaches in a hybrid kinetics embedding (HyKE-Net) framework for dynamic PET reconstruction. We first introduce a novel *hybrid* model of tracer kinetics consisting of a physics-based function augmented by a neural component to account for its gap to data-generating tracer kinetics, both identifiable from data. We then embed this hybrid model at the latent space of an encoding-decoding framework to enable both supervised and unsupervised identification of the hybrid kinetics and thereby dynamic PET reconstruction. Through both phantom and real-data experiments, we demonstrate the benefits of HyKE-Net – especially in unsupervised reconstructions – over existing physics-based and data-driven baselines as well as its ablated formulations where the embedded tracer kinetics are purely physics-based, purely neural, or hybrid but with a non-adaptable neural component.

**Keywords:** Dynamic PET reconstruction · Hybrid modeling.

## 1 Introduction

Dynamic positron emission tomography (PET) imaging is widely used in clinical diagnosis and treatment for elucidating the spatial distribution and kinetics of radiotracer-labeled biological substrates *in-vivo* [1, 11, 16]. Dynamics PET reconstruction aims to reconstruct a temporal series of spatial concentration distribution of the radioactive tracer (tracer activity images) from a series of noisy

sinograms measured by a PET scanner. This reconstruction remains a challenging task due to the complex spatio-temporal nature of the tracer kinetics as well as the high level of noise and low counting statistics in the sinogram measurements [4, 23], all contributing to the ill-posedness of this inverse problem [15].

Compared to static PET reconstruction [2, 7, 10, 19, 22, 24], the importance to leverage the temporal dynamics of the data is well appreciated in dynamic PET reconstruction. While various traditional optimization and inference strategies have been introduced to incorporate temporal prior as constrains for dynamic PET reconstruction [5, 12, 20, 27], recent deep learning solutions have shown state-of-the-art performances and can be categorized into data-driven *vs.* physics-based approaches to modeling the tracer kinetics underlying the data.

The data-driven approaches [9, 13, 21, 26] generally leverage spatio-temporal neural networks to learn kinetic information directly from data. The learning of this *black-box* kinetics, however, neglects potentially valuable prior knowledge about the tracer kinetics and relies heavily on the supervision of the ground truth tracer activity images – the latter are difficult to obtain in practice. Alternatively, physics-based approaches [8, 14] leverage *a priori* tracer kinetic model in known mathematical expressions and focus on estimating its pixel-wise parameters (parametric images) in order to reconstruct tracer activity images. This *white-box* kinetics introduces valuable prior physics to reduce the reliance on data, although the performance of these approaches can decline as the gap between the prior and data-generating kinetics increases. How to effectively leverage physics-based *a priori* kinetic models to remove the reliance on ground-truth tracer activity images, while addressing its unknown gap to data-generating tracer kinetics remains an open question in dynamic PET reconstruction.

In this paper, we answer this important question with a novel *hybrid* kinetics-embedding framework (HyKE-Net) for dynamic PET reconstruction. As outlined in Fig. 1, HyKE-Net has two important innovations. First, we model the tracer kinetics with a novel hybrid expression, in the form of a universal differential equation [17] that consists of both a known mathematical expression of tracer kinetics representing prior knowledge and a neural function representing its gap to actual data-generating tracer kinetics. Second, we embed this hybrid tracer kinetics in the latent space of an encoding-decoding architecture, enabling (through the encoder) separate identification of both its prior physics-based and unknown neural components directly from measured sinograms, while allowing (through the decoder) *unsupervised* training with only a reconstruction objective at the sinogram space without access to the ground-truth tracer activity images.

We evaluated HyKE-Net for both unsupervised and supervised dynamic PET reconstruction on synthetic and real datasets, in comparison to two traditional methods (FBP [2] and Joint-TV [27]) and one data-driven deep-learning method (FBP-Net [21]). We further ablated the use of hybrid kinetics with the use of purely physics-based, purely neural, and hybrid kinetics but with a global neural component in HyKE-Net. The results provide strong evidence for the benefits of embedding hybrid tracer kinetics to integrate rich prior knowledge while allowing for its errors, especially in unsupervised dynamics PET reconstruction.

## 2 Background

**PET Imaging Model:** The relationship between tracer activity images  $\mathbf{x}$  and measured sinograms  $\mathbf{y}^r$  can be described by:

$$\mathbf{y}^r \sim \text{Poisson}(\bar{\mathbf{y}} = \mathbf{D}(\mathbf{G}\mathbf{x}) + \mathbf{n}) \quad (1)$$

where  $\mathbf{G}$  describes the discrete radon transform (*i.e.*, projection),  $\mathbf{D}$  models the detection-probability of the PET scanner, noise matrix  $\mathbf{n}$  represents the expectation of randoms and scatters, and  $\bar{\mathbf{y}}$  the expectation of measured sinograms.

**Tracer Kinetics of Dynamic PET:** Various models have been proposed to model tracer kinetics in dynamic PET. Due to the simple implementation and biological plausibility, we consider the one- and two-tissue compartment models:

$$\begin{aligned} \text{One-tissue: } \dot{C}_{T_i}(t) &= -k_{2i}C_{T_i}(t) + k_{1i}C_P(t) & (2) \\ \text{Two-tissue: } \begin{bmatrix} \dot{C}_{E_i}(t) \\ \dot{C}_{M_i}(t) \end{bmatrix} &= \begin{bmatrix} -k_{2i} - k_{3i} & k_{4i} \\ k_{3i} & -k_{4i} \end{bmatrix} \begin{bmatrix} C_{E_i}(t) \\ C_{M_i}(t) \end{bmatrix} + \begin{bmatrix} k_{1i} \\ 0 \end{bmatrix} C_P(t) \\ C_{T_i}(t) &= C_{E_i}(t) + C_{M_i}(t) & (3) \end{aligned}$$

where  $C_P$  is the arterial concentration of nonmetabolized tracer in plasma,  $C_E$  is the concentration of nonmetabolized tracer in tissue,  $C_M$  is the concentration of the radioisotope-labeled metabolic products in tissue,  $C_T$  is the total concentration of radioactivity in tissue, subscript  $i$  denotes different pixel locations, and  $k_1, k_2, k_3, k_4$  are physical kinetic parameters. The estimated values of these parameters across pixels provide the *parametric images* in PET reconstruction. The *tracer activity image*  $\mathbf{x}_k$  at the  $k$ th time frame can then be computed as:

$$\mathbf{x}_k = \left\{ \frac{1}{t_k - t_{k-1}} \int_{t_{k-1}}^{t_k} [(1 - V_i)C_{T_i}(t) + V_i C_P(t)] e^{-\frac{t}{\tau}} dt \right\}_{i=1:W \times H} \quad (4)$$

where  $\tau$  is the tracer decay coefficient,  $t_k - t_{k-1}$  the scan interval,  $V$  the vascular volume fraction, and  $W$  and  $H$  the width and height of the tracer activity image.

## 3 Methodology

As illustrated in Fig. 1, HyKE-Net has two key design components: 1) an embedded hybrid tracer kinetic model combining a prior physics-based compartment model and an unknown neural function describing errors in prior physics, and 2) an encoding-decoding formulation that bridges this embedding space to the space of tracer activity images and further to the space of measured sinograms, to enable unsupervised identification of hybrid tracer kinetics and thereby unsupervised reconstruction of the time sequence of tracer activity images.

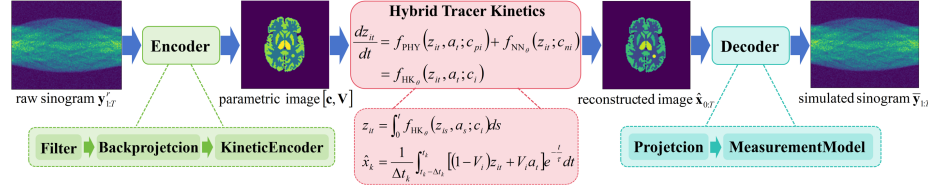


**Fig. 1.** Overview of HyKE-Net with hybrid tracer kinetics in the latent space to facilitate supervised or unsupervised dynamic PET reconstruction.

**Hybrid Tracer Kinetics:** We first describe the tracer kinetics as a hybrid model in the form of a universal differential equation [17], with a physics-based compartment model augmented by a neural kinetic function:

$$\frac{d\mathbf{z}_{it}}{dt} = f_{\text{PHY}}(\mathbf{z}_{it}, a_t; \mathbf{c}_{pi}) + f_{\text{NN}\theta}(\mathbf{z}_{it}; \mathbf{c}_{ni}) = f_{\text{HK}\theta}(\mathbf{z}_{it}, a_t; \mathbf{c}_i) \quad (5)$$

$$\mathbf{z}_{it} = \int_0^t f_{\text{HK}\theta}(\mathbf{z}_{is}, a_s; \mathbf{c}_i) ds \quad (6)$$

where  $f_{\text{PHY}}(\mathbf{z}_{it}, a_t; \mathbf{c}_{pi})$  represents either the one- or two-tissue compartment model introduced in Equations (2)-(3),  $a(t) = C_P(t)$ , and  $\mathbf{c}_{pi}$  include its physical kinetic parameters.  $f_{\text{NN}\theta}(\mathbf{z}_{it}; \mathbf{c}_{ni})$  is a neural network parameterized by  $\theta$ , intended to account for the gap between the prior and data-generating tracer kinetics: instead of assuming a single neural function  $f_{\text{NN}\theta}(\mathbf{z}_{it})$  globally shared by all training sequences, we assume that it can vary with the training samples and set it conditioned on an additional abstract neural kinetic parameter  $\mathbf{c}_{ni}$ .  $\mathbf{c}_{pi}$  and  $\mathbf{c}_{ni}$  ( $[\mathbf{c}_{pi}, \mathbf{c}_{ni}] = \mathbf{c}_i$ ) will be inferred from individual sequences to allow the identification of hybrid tracer kinetics. The generation of tracer activity images  $\mathbf{x}_{1:T}$  from  $\mathbf{z}_{it}$  is as described in Equation (4), in which  $V_i$  will also be inferred.

**Identification of Hybrid Tracer Kinetics:** To infer kinetic parameters  $[\mathbf{c}_i, V_i]$  from measured sinograms, instead of a purely neural encoder, we consider a hybrid encoder that transforms from the sinogram domain to image domain by a physics-embedded process. Inspired by the FBP algorithm [2], this is achieved via a filtering process with a learnable spatial filter  $h_\phi(\cdot)$  parameterized by  $\phi$  and a backprojection process with a backprojection matrix  $\mathbf{G}^T$ :

$$\tilde{\mathbf{x}}_{1:T} = \mathbf{G}^T(h_\phi(\mathbf{y}_{1:T}^r)) \quad (7)$$

We then utilize a kinetic encoder  $g_\varphi(\cdot)$  with parameters  $\varphi$  to infer kinetic parameter of each pixel (parametric images) as:

$$[\hat{\mathbf{c}}, \hat{\mathbf{V}}] = g_\varphi(\tilde{\mathbf{x}}_{1:T}), \quad \hat{\mathbf{c}} = \{\hat{\mathbf{c}}_i\}_{1:N}, \quad \hat{\mathbf{V}} = \{\hat{V}_i\}_{1:N} \quad (8)$$

**Supervised and Unsupervised Reconstructions:** Given inferred parameters  $[\hat{\mathbf{c}}, \hat{\mathbf{V}}]$ , the tracer activity images  $\hat{\mathbf{x}}_{1:T}$  can be reconstructed by Equations

(4)-(6). If ground truth  $\mathbf{x}_{1:T}$  are available, we can optimize HyKE-Net with a supervised objective as the mean squared error (MSE) between  $\mathbf{x}_{1:T}$  and  $\hat{\mathbf{x}}_{1:T}$ :

$$\arg \min_{\theta, \phi, \varphi} \mathcal{L}_s = \|\mathbf{x}_{1:T} - \hat{\mathbf{x}}_{1:T}\|_2^2 + \lambda \|\hat{\mathbf{x}}_{1:T} - \tilde{\mathbf{x}}_{1:T}\|_2^2 \quad (9)$$

where the second regularization term provides additional constraints for  $\tilde{\mathbf{x}}_{1:T}$  obtained in Equation (7) to be similar to reconstructed images  $\hat{\mathbf{x}}_{1:T}$ . If ground-truth  $\mathbf{x}_{1:T}$  are not available, we further obtain the reconstructed sinograms  $\bar{\mathbf{y}}_{1:T}$  from  $\hat{\mathbf{x}}_{1:T}$  using the projection and measurement model as described in Equation (1), and formulate the unsupervised objective as the negative Poisson log-likelihood on  $\bar{\mathbf{y}}_{1:T}$  with the same regularization term used in Equation (9):

$$\arg \min_{\theta, \phi, \varphi} \mathcal{L}_u = -(\mathbf{y}_{1:T}^r \log \bar{\mathbf{y}}_{1:T} - \bar{\mathbf{y}}_{1:T}) + \lambda \|\hat{\mathbf{x}}_{1:T} - \tilde{\mathbf{x}}_{1:T}\|_2^2 \quad (10)$$

We choose the use of physics-based functions to bridge between the sinogram and image space, both in encoding (Equation (7)) and decoding (Equation (1)), to avoid the need of a large neural network for accommodating the size of PET images and sinograms ( $128 \times 128$  and  $160 \times 128$ , respectively, in our experiments).

## 4 Experiments and Results

### 4.1 Experiments on Synthetic Data

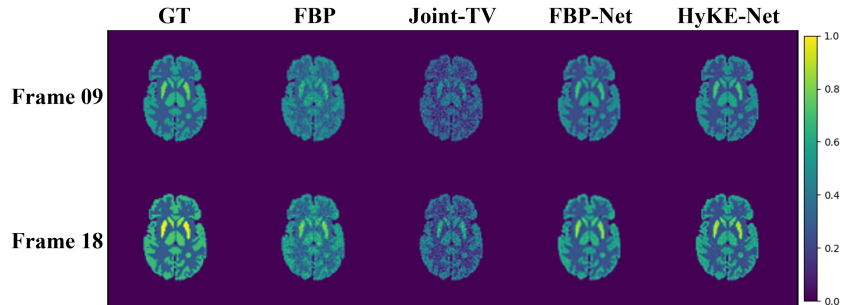
**Data:** We used the  $128 \times 128$  2D Zubal brain phantom [28] with a tumor added. The phantom contained 6 regions of interests (ROIs) and the scanning schedule included 18 frames over 60 min as  $3 \times 60$  s,  $9 \times 180$  s,  $6 \times 300$  s. A two-tissue compartmental model with Feng’s input function [6] was used to generate ground-truth kinetic  $^{18}\text{F}$ -FDG scans, with its kinetic parameters selected randomly from Gaussian distributions as described in [21]. The projection processes were performed following [18], with 160 projection angles, 128 detector bins, 20% Poisson random noise, and a total photon-count of around  $1.8 \times 10^7$ . Scattered photons were not considered. We generated a total of 400 pairs of tracer activity images and sinograms: 320 for training, 40 for validation, and 40 for testing.

**Models and Metrics:** We utilized one-tissue compartment model as described in Equation (2) as prior physics  $f_{\text{PHY}}$  to induce an inherent gap to the data-generating two-tissue compartment model. The neural kinetic function  $f_{\text{NN},\theta}$ , spatial filter  $h_\phi$ , and kinetics encoder  $g_\varphi(\cdot)$  were modeled as a simple fully-connected network, a residual CNN [25], and a 3D-Unet [3] respectively. For quantitative evaluation, we considered peak signal-to-noise ratio (PSNR) and structural similarity (SSIM) for the activity image and MSE in the ROIs.

**Comparison with Existing Baselines:** We compared HyKE-Net with three existing methods including traditional direct reconstruction (FBP) [2], traditional kinetics-constrained reconstruction (Joint-TV) [27], and deep learning

**Table 1.** Comparison of HyKE-Net with baselines on phantom data.

	Unsupervised Reconstruction			Supervised Reconstruction		
	MSE( $e^{-2}$ ) ↓	PSNR ↑	SSIM ↑	MSE( $e^{-2}$ ) ↓	PSNR ↑	SSIM ↑
FBP	2.25(0.00)	12.85(0.00)	0.41(0.00)	/	/	/
Joint-TV	5.61(0.00)	18.69(0.00)	0.69(0.00)	/	/	/
FBP-Net	1.43(0.01)	23.76(0.31)	0.91(0.00)	0.05(0.01)	40.02(0.70)	0.98(0.00)
HyKE-Net	<b>0.75(0.00)</b>	<b>27.90(0.35)</b>	<b>0.94(0.00)</b>	<b>0.03(0.01)</b>	<b>42.33(0.73)</b>	<b>0.98(0.00)</b>

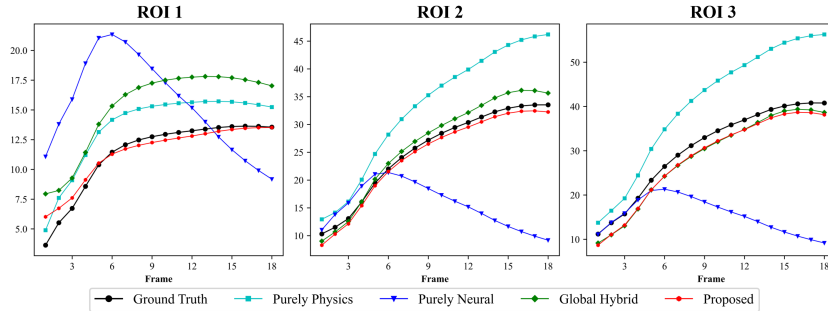
**Fig. 2.** Examples of unsupervised reconstruction results from HyKE-Net and baselines.

based reconstruction with spatial-temporal neural networks (FBP-Net) [21]. While FBP-Net is supervised in its original formulations, we added our decoder in Equation (1) to test its performance in unsupervised reconstruction in comparison to the rest of the models. Quantitative results are summarized in Table 1 and visual examples of all ROIs are provided in Fig. 2. While HyKE-Net’s performance was moderately stronger than FBP-Net in supervised settings, it significantly outperformed all baselines in unsupervised settings. These suggest that, when ground-truth tracer activity images are not available to supervise the training, the use of hybrid kinetics brings significant benefits compared to purely physics-based (as in Joint-TV) or data-driven kinetics (as in FBP-Net).

**Ablation of the Benefits of Hybrid Kinetics:** We further ablated the benefits of embedding hybrid kinetics by comparing the proposed HyKE model with the following three alternatives while keeping the rest of the framework identical: 1) purely physics kinetics:  $\frac{dz_{it}}{dt} = f_{\text{PHY}}(z_{it}, a_t; \mathbf{c}_{pi})$ ; 2) purely neural kinetics:  $\frac{dz_{it}}{dt} = f_{\text{NN}\theta}(z_{it}; \mathbf{c}_{ni})$ ; and 3) global hybrid kinetics:  $\frac{dz_{it}}{dt} = f_{\text{PHY}}(z_{it}, a_t; \mathbf{c}_{pi}) + f_{\text{NN}\theta}(z_{it})$  where the neural component  $f_{\text{NN}\theta}$  is shared across all samples. Quantitative results are summarized in Table 2 and examples of unsupervised reconstruction of the time activity curve (TAC) in three ROIs are shown in Fig. 3. As demonstrated, both purely physics-based and purely neural kinetics struggle to reconstruct the data-generating kinetics. The use of global hybrid kinetics helps (green), but can be further improved by a hybrid kinetics model adaptable to the data as in HyKE to consider the heterogeneous errors in the prior physics.

**Table 2.** Ablating the benefits of hybrid kinetics with an adaptive neural component.

	Unsupervised Reconstruction			Supervised Reconstruction		
	MSE( $e^{-2}$ ) ↓	PSNR ↑	SSIM ↑	MSE( $e^{-2}$ ) ↓	PSNR ↑	SSIM ↑
Purely Physics	5.97(0.36)	18.89(0.27)	0.63(0.03)	0.07(0.00)	38.10(0.01)	0.97(0.00)
Purely Neural	19.55(0.21)	13.74(0.05)	0.61(0.01)	0.04(0.01)	41.14(0.12)	0.98(0.00)
Global Hybrid	1.39(0.04)	25.22(0.12)	0.92(0.02)	0.04(0.00)	40.72(0.58)	0.98(0.00)
HyKE-Net	<b>0.75(0.00)</b>	<b>27.90(0.35)</b>	<b>0.94(0.00)</b>	<b>0.03(0.01)</b>	<b>42.33(0.73)</b>	<b>0.98(0.00)</b>

**Fig. 3.** Examples of unsupervised reconstruction of time activity curves.

## 4.2 Experiments on Real Data

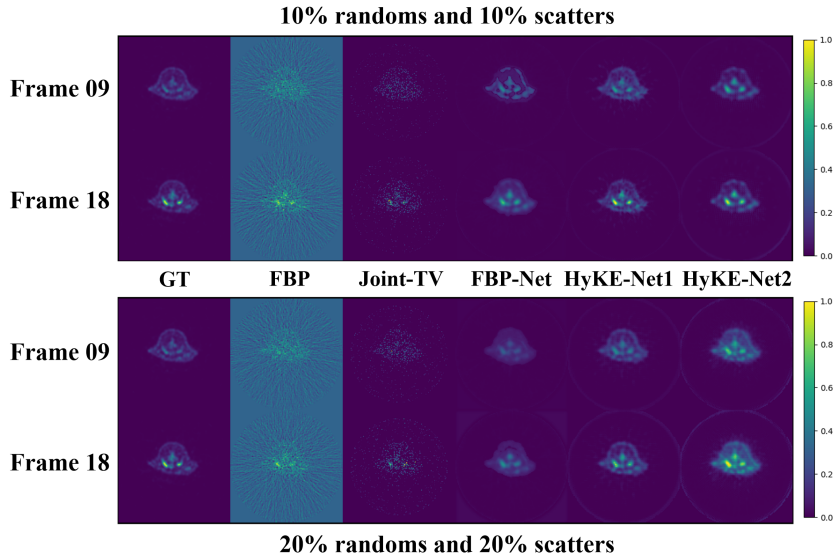
**Data & Models:** Animal data were obtained from those described in [21]. The sampling protocol for dynamic PET scans was set to  $3 \times 60$  s,  $9 \times 180$  s,  $6 \times 300$  s. The ground-truth  $\mathbf{x}_{1:T}$  were reconstructed with CT attenuation correction and full 3D counts. Due to the lack of access to the CT images and thus the inability to properly model the actual sinogram measurement process, we simulated low-count sinograms with  $2.4 \times 10^5$  photon-count with different levels of randoms and scatters: we tested how HyKE-Net and its baselines responds to these noises in the data when the measurement model is unaware of these noises. Note that the data-generating tracer kinetics underlying  $\mathbf{x}_{1:T}$  is not known, which is the main motivation for HyKE-Net. 600 images from 10 rates were used, with eight rats selected randomly for training, one for validation, and one for testing.

Since real  $C_p(t)$  (or  $a_t$ ) is not available in real data, we used  $C_p$  from synthetic-data experiments but also provided it as an input to the neural kinetic function  $f_{NN_\theta}(\mathbf{z}_{it}, a_t; \mathbf{c}_{ni})$  to allow the modeling of its errors. We compared HyKE-Net with existing baselines for unsupervised reconstruction considering 10% *vs.* 20% randoms and scatters in the measured sinograms. Because the data-generating kinetics is unknown, we further tested the effect of using the one-tissue *vs.* two-tissue compartment model as prior physics in HyKE-Net (noted as HyKE-Net1 and HyKE-Net2 respectively).

**Results:** The quantitative results are summarized in Table 3 with visual examples shown in Fig. 4. While all methods' performance decreased as the noises in

**Table 3.** Comparison of HyKE-Net with baselines on real data.

	10% randoms and 10% scatters			20% randoms and 20% scatters		
	MSE( $e^{-3}$ ) ↓	PSNR ↑	SSIM ↑	MSE( $e^{-3}$ ) ↓	PSNR ↑	SSIM ↑
FBP	80.00(0.00)	10.97(0.00)	0.03(0.00)	84.05(0.00)	10.75(0.00)	0.03(0.00)
Joint-TV	1.73(0.00)	27.63(0.00)	0.31(0.00)	1.84(0.00)	27.35(0.00)	0.31(0.00)
FBP-Net	0.24(0.02)	36.24(0.42)	0.60(0.01)	0.42(0.05)	33.82(0.48)	0.55(0.03)
HyKE-Net1	0.23(0.01)	36.12(0.68)	0.61(0.00)	<b>0.26(0.02)</b>	<b>36.93(0.43)</b>	<b>0.60(0.01)</b>
HyKE-Net2	<b>0.22(0.02)</b>	<b>36.71(0.50)</b>	<b>0.61(0.00)</b>	0.32(0.05)	34.91(0.43)	0.58(0.00)

**Fig. 4.** Examples of unsupervised reconstruction results on real data.

the sinograms (and thus the errors in the measurement model) increased, HyKE-Net consistently outperformed its baselines in both settings. In particular, when using the one-tissue compartment model as the prior physics, HyKE-Net demonstrated a strong robustness to measurement errors compared to all baselines. Interestingly, when using a more sophisticated two-tissue compartment model, the performance of HyKE-Net showed marginal improvements given lower measurement errors but faster deterioration given higher measurement errors – this may suggest that, when measurement quality is low, a more complex physics-based kinetics model may increase the difficulty of identifiability.

## 5 Conclusion

We present a novel framework HyKE-Net for dynamic PET reconstruction that embeds hybrid tracer kinetics into a physics-based encoding-decoding architecture. Experiment on synthetic data and real data demonstrated its benefits from

integrating rich prior knowledge while allowing for its errors, especially in unsupervised dynamic PET reconstruction. Future work will focus on addressing the increased computational cost of HyKE-Net due to hybrid modeling, and the impact on unsupervised reconstruction by the errors in the measurement model – including the possibility to make the measurement model hybrid. Future works will also focus on extensive quantitative evaluations on real human data.

**Acknowledgements.** This work is supported in part by the National Key Research and Development Program of China (No: 2020AAA0109502); the Talent Program of Zhejiang Province (No: 2021R51004); NIH NHLBI grant R01HL145590 and NSF OAC-2212548.

## References

1. Boss, D.S., Olmos, R.V., Sinaasappel, M., Beijnen, J.H., Schellens, J.H.: Application of pet/ct in the development of novel anticancer drugs. *The oncologist* **13**(1), 25–38 (2008)
2. Brooks, R.A., Di Chiro, G.: Statistical limitations in x-ray reconstructive tomography. *Medical physics* **3**(4), 237–240 (1976)
3. Çiçek, Ö., Abdulkadir, A., Lienkamp, S.S., Brox, T., Ronneberger, O.: 3d u-net: learning dense volumetric segmentation from sparse annotation. In: *Medical Image Computing and Computer-Assisted Intervention–MICCAI 2016: 19th International Conference, Athens, Greece, October 17–21, 2016, Proceedings, Part II* 19. pp. 424–432. Springer (2016)
4. Cui, J., Qin, Z., Chen, S., Chen, Y., Liu, H.: Structure and tracer kinetics-driven dynamic pet reconstruction. *IEEE Transactions on Radiation and Plasma Medical Sciences* **4**(4), 400–409 (2019)
5. Cui, J., Qin, Z., Chen, S., Chen, Y., Liu, H.: Structure and tracer kinetics-driven dynamic pet reconstruction. *IEEE Transactions on Radiation and Plasma Medical Sciences* **4**(4), 400–409 (2019)
6. Feng, D., Huang, S.C., Wang, X.: Models for computer simulation studies of input functions for tracer kinetic modeling with positron emission tomography. *International journal of bio-medical computing* **32**(2), 95–110 (1993)
7. Fessler, J.A.: Penalized weighted least-squares image reconstruction for positron emission tomography. *IEEE transactions on medical imaging* **13**(2), 290–300 (1994)
8. Gong, K., Catana, C., Qi, J., Li, Q.: Direct reconstruction of linear parametric images from dynamic pet using nonlocal deep image prior. *IEEE Transactions on Medical Imaging* **41**(3), 680–689 (2021)
9. Hu, R., Cui, J., Li, C., Yu, C., Chen, Y., Liu, H.: Dynamic low-count pet image reconstruction using spatio-temporal primal dual network. *Physics in Medicine and Biology* (2023)
10. Hudson, H.M., Larkin, R.S.: Accelerated image reconstruction using ordered subsets of projection data. *IEEE transactions on medical imaging* **13**(4), 601–609 (1994)
11. Kostakoglu, L., Agress Jr, H., Goldsmith, S.J.: Clinical role of fdg pet in evaluation of cancer patients. *Radiographics* **23**(2), 315–340 (2003)
12. Leahy, R.M., Qi, J.: Statistical approaches in quantitative positron emission tomography. *Statistics and Computing* **10**, 147–165 (2000)

13. Li, S., Wang, G.: Deep kernel representation for image reconstruction in pet. *IEEE transactions on medical imaging* **41**(11), 3029–3038 (2022)
14. Li, Y., Hu, J., Sari, H., Xue, S., Ma, R., Kandarpa, S., Visvikis, D., Rominger, A., Liu, H., Shi, K.: A deep neural network for parametric image reconstruction on a large axial field-of-view pet. *European journal of nuclear medicine and molecular imaging* **50**(3), 701–714 (2023)
15. Liu, H., Gao, F., Guo, M., Xue, L., Nie, J., Shi, P.: Pet image reconstruction: mean, variance, and optimal minimax criterion. *Journal of Physics D: Applied Physics* **48**(15), 155401 (2015)
16. Machac, J.: Cardiac positron emission tomography imaging. In: *Seminars in nuclear medicine*. vol. 35, pp. 17–36. Elsevier (2005)
17. Rackauckas, C., Ma, Y., Martensen, J., Warner, C., Zubov, K., Supekar, R., Skinner, D., Ramadhan, A., Edelman, A.: Universal differential equations for scientific machine learning. arXiv preprint arXiv:2001.04385 (2020)
18. Ronchetti, M.: Torchradon: Fast differentiable routines for computed tomography. arXiv preprint arXiv:2009.14788 (2020)
19. Shepp, L.A., Vardi, Y.: Maximum likelihood reconstruction for emission tomography. *IEEE transactions on medical imaging* **1**(2), 113–122 (1982)
20. Tong, S., Alessio, A., Kinahan, P., Liu, H., Shi, P.: A robust state-space kinetics-guided framework for dynamic pet image reconstruction. *Physics in Medicine & Biology* **56**(8), 2481 (2011)
21. Wang, B., Liu, H.: Fbp-net for direct reconstruction of dynamic pet images. *Physics in Medicine & Biology* **65**(23), 235008 (2020)
22. Wang, G., Qi, J.: Penalized likelihood pet image reconstruction using patch-based edge-preserving regularization. *IEEE transactions on medical imaging* **31**(12), 2194–2204 (2012)
23. Wernick, M.N., Infusino, E.J., Milosevic, M.: Fast spatio-temporal image reconstruction for dynamic pet. *IEEE transactions on medical imaging* **18**(3), 185–195 (1999)
24. Xie, N., Gong, K., Guo, N., Qin, Z., Wu, Z., Liu, H., Li, Q.: Penalized-likelihood pet image reconstruction using 3d structural convolutional sparse coding. *IEEE Transactions on Biomedical Engineering* **69**(1), 4–14 (2020)
25. Yang, W., Zhang, H., Yang, J., Wu, J., Yin, X., Chen, Y., Shu, H., Luo, L., Coatrieux, G., Gui, Z., et al.: Improving low-dose ct image using residual convolutional network. *Ieee Access* **5**, 24698–24705 (2017)
26. Yokota, T., Kawai, K., Sakata, M., Kimura, Y., Hontani, H.: Dynamic pet image reconstruction using nonnegative matrix factorization incorporated with deep image prior. In: *Proceedings of the IEEE/CVF International Conference on Computer Vision*. pp. 3126–3135 (2019)
27. Yu, H., Chen, S., Chen, Y., Liu, H.: Joint reconstruction of dynamic pet activity and kinetic parametric images using total variation constrained dictionary sparse coding. *Inverse Problems* **33**(5), 055011 (2017)
28. Zubal, I.G., Harrell, C.R., Smith, E.O., Rattner, Z., Gindi, G., Hoffer, P.B.: Computerized three-dimensional segmented human anatomy. *Medical physics* **21**(2), 299–302 (1994)